Estimating Sit-to-Stand Dynamics Using a Single Depth Camera

Robert Peter Matthew, Sarah Seko, Jeannie Bailey, Ruzena Bajcsy, and Jeffrey Lotz

***Abstract*—Kinetic and dynamic motion analysis provides quantitative, functional assessments of human ability that are unobtainable through static imaging methods or subjective surveys. While biomechanics facilities are equipped to perform this measurement and analysis, the clinical translation of these methods is limited by the specialized skills and equipment needed. This paper presents and validates a method for estimating dynamic effects such as joint torques and body momenta using a single depth camera. An allometrically scaled, sagittal plane dynamic model is used to estimate the joint torques at the ankles, knees, hips, and low back, as well as the torso momenta, and shear and normal loads at the L5-S1 disk. These dynamic metrics are applied to the sit-to-stand motion and validated against a gold-standard biomechanical system consisting of full-body active motion-capture and force-sensing systems. The metrics obtained from the proposed method were found to have excellent concordance with peak metrics that are consistent with prior biomechanical studies. This suggests the feasibility of using this system for rapid clinical assessment, with applications in diagnostics, longitudinal tracking, and quantifying patient recovery.**

***Index Terms*—Depth-camera, rigid-body model, dynamics, sit-to-stand, biomechanics, lower lumbar loads.**

I. Introduction

FUNCTIONAL assessment measures enable the quantitative assessment of patient ability. While methods such as static radiographs and goniometry quantify posture or range of motion at a joint level, functional assessments allow for insight into patient independence by gauging task level performance [1].

The clinical deployment of biomechanical motion assessment is limited by the required hardware, time, and expertise. Musculoskeletal analysis is typically performed in dedicated laboratory spaces, using specialist motion-capture and force-sensing systems. Tracked motions of surface markers are used to estimate the rigid-body motions of the underlying skeletal system. This inverse kinematics process allows for the decomposition of complex limb motions into constituent joint trajectories. A dynamic model can then be used to determine the joint torques required to produce these joint trajectories. The dynamic parameters of these models can be allometrically scaled from population data [2]–[5], or can be estimated in vivo using identification techniques [6], [7]. This analysis can be validated by measuring the contact forces exerted by the subject. Myography techniques such as surface electro-myograpy and acoustic-myography can be used to estimate muscle activation. These activation patterns can be compared to torque estimates found through inverse dynamic methods [8], [9].

While detailed musculoskeletal models for processing motion data exist [10], [11], current clinical measures of lower limb and spine function rely on timing simple activities such as standing from sitting or walking a known distance [12]. The cost and complexity of deploying more complicated systems has resulted in a disparity between the analysis conducted in speciality biomechanics research facilities and the existing standards of clinical care.

The use of sensorised wearable devices for monitoring occupational tasks and rehabilitation has been explored as a method for overcoming this gap. Garments instrumented with Inertial Measurement Units have been developed to regulate postural control [13], track the curvature of the spine [14], or warn users of poor posture when performing lifting tasks [15]. These wearable systems offer the potential to track a set of key movement parameters. The assessment and feedback, however, is limited to angular estimates of the spine. More detailed biomechanical systems have been developed such as the Lumbar Motion Monitor [16]. This exoskeletal system tracks the kinematics and kinetics of the thoracolumbar spine during a specific occupational or assessment task [17]. The shear and compressive forces in the spine can then be estimated by combining the tracked spine movements with motion capture and surface myography [18]. This approach is limited by dedicated hardware requirements.

A number of vision-based human motion tools have been developed [19]. The Microsoft Kinect can be used to estimate joint centres from a colour and depth image using a pixel classification approach [20]. While these estimates are noisy and can be inaccurate in cases of self-occlusion [21], the system is able to provide real-time estimates which have been used for biomechanical assessments of movement [22]. There are alternative methods for reconstructing human motion from single or multiple cameras, with a number of improvements in accuracy over a wide range of real-world situations. These methods often use template surface models [23], [24] or pixel/voxel

Manuscript received October 3, 2018; revised November 16, 2018; accepted December 21, 2018. Date of publication February 4, 2019; date of current version November 6, 2019. This work was supported by SBIR with Grant 1R41AR068202-01A1. *(Corresponding author: Robert Peter Matthew.)*

R. P. Matthew, S. Seko, and R. Bajcsy are with the Department of Electrical Engineering and Computer Science, University of California at Berkeley, Berkeley, CA 94720 USA (e-mail: rpmatthew@berkeley.edu; seko@berkeley.edu; bajcsy@berkeley.edu).

J. Bailey and J. Lotz are with the Department of Orthopaedic Surgery, University of California at San Francisco, San Francisco, CA 94143 USA (e-mail: jeannie.bailey@ucsf.edu; Jeffrey.Lotz@ucsf.edu).

Digital Object Identifier 10.1109/JBHI.2019.2897245

classification-based machine learning [25]–[28]. While appearing promising, the validation of these approaches is lacking when compared to conventional biomechanical studies. Zhang [29] presented a method for estimating kinematic and dynamic states from a combination of three depth cameras and force sensing shoes. Re-projected marker error was the only quantitative measure used for validation, with the estimated contact forces and joint torques only compared qualitatively. This is compared to the kinematic and dynamic assessments performed by Corazza [30] and Anderson [31]. These studies compare joint angles, contact forces, and muscle activation estimates against gold-standard motion capture, force platforms, and electromyography systems.

A recent study by Plantard [32] demonstrated the utility of the Kinect as assessment system for the ergonomic evaluation of upper limb tasks. The raw Kinect was filtered by comparing the observed data with a known database of actions [33]. This filtered Kinect data was then combined with an allometrically scaled upper limb dynamic model [5] to estimate the corresponding joint torques. This method was found to provide reliable estimates of shoulder torques for a box-handling task, including cases with occlusion.

A. Sit to Stand

The Five-Times-Sit-to-Stand (FT-STS) is a standard clinical assessment for individuals with balance disorders and lower limb weakness [12]. The clinical FT-STS consists of performing five repeated standing and sitting actions as fast as possible. The subjects arms are crossed on their chest and the total time for the five actions is measured on a stopwatch. The total time is then compared against a set of thresholds which can indicate increased disability, morbidity or likelihood of falling [34], [35].

The FT-STS has been found to discriminate subjects with balance disorders, but time alone may not sufficiently capture changes in ability. Other threshold based tests and written questionnaires such as the Activities-specific Balance Confidence scale [36] and the Dynamic Gait Index [37] have been shown to be better at discriminating balance disorders [38].

The dynamics and biomechanics of the STS action have been explored, with a number of proposed dynamic models used to describe the transition of the subject to a stable standing position. These models typically examine the locations of the effective Centre of Mass (CoM) and the Base of Support (BoS) to estimate the subject's stability. Riley [39] studied the motions of healthy subjects and separated the standing action into four separate phases of *momentum-transfer* standing:

I. flexion-momentum is the initial rotation of the hips and pelvis forward. This phase ends with *seat-off*, where weight transfers from the chair to the feet.

II. momentum-transfer consists of the forward momentum of the CoM being converted into vertical momentum.

III. vertical extension is the vertical rise of the CoM to a standing position.

IV. stabilisation consists of settling of any postural sway in the CoM.

At seat-off (the transition between phase I. and II.), people are typically statically unstable. To transition to standing, healthy subjects typically generate forward momentum by swinging their torso forward. This forward momentum helps move the CoM over the BoS dynamically, allowing the person to then rise to move through the statically unstable region into a standing posture [39]. In contrast, it has been shown that elderly subjects can adopt a *stabilisation* strategy [40], during which the CoM is shifted over the BoS through an exaggerated torso lean. This leaning action can reduce or completely bypass any statically unstable portion of the standing action.

Dynamic analysis of failed STS motions has been performed. Riley [41] found that both *sit-back* and *step* failures were linked with weakness or poor balance control. Both of these failure modes were found to be less energetic, with decreased linear and sagittal plane angular momentum. Age did not significantly affect hip and knee torque when moving at self selected speeds [42] in healthy elderly and young female populations. BMI has been found to influence torque distributions, with obese subjects having higher peak knee torques than hip torques [43]. Subjects with Parkinson's disease have been found to have decreased hip flexion torques when performing STS [44]. Combined with the decreased horizontal and vertical forces, this suggests that subjects with Parkinson's disease may rely less on momentum transfer due to difficulties in coordinating synchronised body motion. These studies demonstrate the importance of developing a clinically deployable system for computing sagittal dynamics.

B. Contributions

This paper introduces a fast method for performing full-body contactless dynamic analysis of the STS action using a single depth camera. Building on the author's prior results in improving the accuracy of the Kinect for STS actions by imposing rigid-body constraints [45], this work adds reduced-complexity allometrically-scaled dynamic and musculoskeletal models. This provides estimates of torso momenta and joint torques of the low back, and lower limbs, key metrics that have been shown to act as correlates of disability in patient populations. The incorporation of a low back model adds the ability to perform loading analysis at a common site of injury and chronic pain.

The accuracy and concordance of these measures are assessed against gold-standard biomechanical systems such as full-body motion capture and force plates. The proposed system was found to have high concordance and accuracy compared to the gold-standard measures supporting its use as a method of motion assessment.

This analysis is performed for a standard clinical test with minimal additional equipment reducing the need for a dedicated motion analysis facility or specialists to conduct and analyse the experimental data. While the computational rate of 25 fps is *almost* real time, this number is based on unoptimised code running in MATLAB. Improvements to the code such as running the inverse dynamics step in parallel, or an implementation in C++ should increase computation rate.

II. Modelling Framework

The dynamic and musculoskeletal recovery process consists of several steps. First, a filtered rigid-body estimate of ankle, knee, hip, and low-back joint angles are found in the sagittal

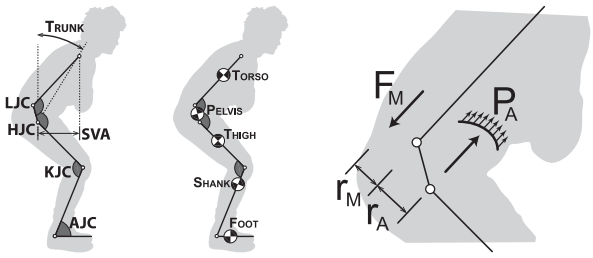

Fig. 1. Left: Simplified five segment rigid-body kinematic model in the sagittal plane. The serial chain structure is connected by joints at the ankle (AJC), knee (KJC), hip (HJC), and at the lower lumbar L5-S1 (LJC). Two position metrics are also shown, the trunk inclination angle from the vertical, and the Sagittal Vertical Axis (SVA). The SVA is defined as the horizontal distance between the shoulder and hip centres in the sagittal plane. Middle: Dynamic model used in this analysis. Each of the five body segments are modelled as being an inertial mass. Right: Low back model. The torque found from the inverse dynamic analysis is used to estimate the effective forces from the low back extensor muscles F_M and the Intra-Abdominal Pressure (IAP) P_A.

plane. These angles and their associated derivatives are combined with a height and mass scaled allometric model to find estimates of the corresponding joint torques and contact forces via inverse dynamics. Special attention is given to the low-back, with the contact wrench used to estimate the corresponding muscular forces and abdominal pressures. The total forces at the low-back are combined to estimate the shear and compressive forces acting at the L5-S1 disc.

A. Prior Data: Kinematics

The four link rigid-body dynamic model used in this work requires a smooth set of input joint angles. A number of methods can be used to obtain these angles from image and depth camera data, or alternative sensors. This paper uses an allometrically scaled rigid-body model and an unscented Kalman filter to post-process raw Kinect 2 joint centre data. This method was chosen for the fast computation rate (524 fps) and the availability of commercial depth camera systems which can estimate the location of joint centres from a RGB-Depth image. The full kinematic recovery process is presented in the associated kinematic validation paper [45]. A brief overview is given below for completeness.

The Kinect uses a pixel labelling strategy to estimate joint centre locations. Machine learning is used to label any pixels containing a limb segment found in the image [20]. The intersections between these labelled segments are then used to infer the corresponding joints centres. This process does not enforce rigid-body constraints, resulting in an estimated skeleton with varying limb lengths that is sensitive to occlusion. This sensitivity can be problematic in cases of self-occlusion, such as when a subject's knees occlude the hips during sitting.

To correct for this, the raw Kinect joint estimates are taken to be noisy measurements of the true joint locations. An unscented Kalman filter is used to enforce rigid body constraints by combining an allometrically scaled kinematic model with a model of the expected error in the Kinect joint centre estimates (Figure 1). In cases of occlusion, joint positions can be inferred based on these rigid body constraints and motion limits.

The location of the lower-lumbar joint centre (LJC) is estimated to be at the L5-S1 disc level. This single point of rotation is used to represent the relative movement between the pelvis and torso and is based on the approach developed by Anderson et al. [46]. Anderson proposed developing a model for lower lumbar rhythm, estimating the sacral rotation form the torso and knee angles. While this model is widely used in reduced order biomechanical models [4], the model is generated from four subjects performing a box lifting task. As the lumbar rhythm may be dependent on the performed motion [47], a model for lumbar rhythm for STS was developed. This model estimates the location of the LJC based on the estimates of the shoulder (SJC), hip (HJC), knee (KJC), and ankle (AJC) joint centres.

B. Dynamic Model

An allometrically scaled rigid-body dynamic model was used to perform the inverse dynamic analysis required to estimate the contact wrenches at each joint. Each limb segment is modelled as an inertial mass, with the upper limbs fixed in the torso frame (Figure 1). The allometric relationships for segment length (L_i) and mass (m_i) are presented in Table I along with the associated segment centres of mass and radii of gyration. The segment conventions are based on the linkage structure used by Dumas [5]. There are a few differences in the derived model, with some of the segment lengths and terminal ends being changed to be consistent with the *ground-up* model. For a few of these links, joint centres and body segment inertial parameters were recomputed directly from the original source data (McConville [2] and Young [3]).

C. Recursive Formulae for Inverse Dynamics

The Lie group form of the recursive Newton-Euler equations (as presented by Park [48]) were used to convert the estimated joint states into estimated body segment kinetics and contact wrenches. Body frame velocities and accelerations are propagated forward from the base segment to the distal ends of each link. The body segment kinetics are then propagated backwards to obtain the wrench at each joint. For the full definitions on the underlying Lie group notation used, please see Appendix.

The coordinates of a point $\boldsymbol{p}$ written in rigid-body frames A and B can be expressed by the homogeneous transform $\boldsymbol{g}_{AB}$:

$$\boldsymbol{p}_A = \boldsymbol{g}_{A,B}\boldsymbol{p}_B \tag{1}$$

1) Forward Propagation: Using this notation, the forward propagation of body frame velocities $\boldsymbol{V}$ and accelerations $\dot{\boldsymbol{V}}$ between the previous link $i-1$ and current link i can be found. The updated rigid-body transformation between the two links can be written:

$$\boldsymbol{g}_{i-1,i} = \boldsymbol{g}_{\boldsymbol{0}i-1,i}e^{\hat{\boldsymbol{\xi}}_i\theta_i} \tag{2}$$

where $\boldsymbol{\xi}_i$ is the unit screw axis of rotation and θ is the magnitude of the transformation (in this case angle) between the initial frame $\boldsymbol{g}_0$ and its new configuration. The Adjoint mapping $\boldsymbol{Ad}$ can be used find the updated body segment velocities

TABLE I

DYNAMIC MODEL PARAMETERS. MALE VALUES ARE PRESENTED AS THEIR DIFFERENCE FROM THE FEMALE VALUES. SEGMENT LENGTHS (L_i) AND MASSES (m_i) ARE PRESENTED AS FRACTIONS OF THE TOTAL HEIGHT (H) AND MASS (M) OF THE SUBJECT. THE SAGITTAL PLANE POSITION OF THE CENTRE OF MASS AND RADIUS OF GYRATION ARE ALSO PRESENTED AS PERCENTAGES OF THE ASSOCIATED SEGMENT LENGTH. MHI AND MHV ARE THE FIRST AND FIFTH METATARSAL HEADS, MH2 AND MH5 ARE THE SECOND AND FIFTH METACARPAL HEADS.

Segment	Length Definition	Origin	Sex	Length (% of H)	Mass (% of M)	Centre of Mass Y (% of L_i)	Centre of Mass Z (% of L_i)	Radius of Gyration X (% of L_i)
Foot	AJC to mid MHI-MHV	ANK	F	6.61	2.0	41.78	9.02	54.3
			M	+1.11	+0.4	+9.02	+13.47	-10.2
Shank	AJC to KJC	ANK	F	KJC - AJC	9.0	-4.88	59.64	28
			M		+0.6	+0.04	-0.65	+0
Thigh	KJC to HJC	KNE	F	HJC-KJC	29.2	-7.65	57.18	32
			M		-4.6	+3.48	+5.09	-2
Pelvis	HJC to LJC	HIP	F	L5S1-HJC	14.6	-12.49	80.36	79
			M		-0.4	-1.56	-4.54	+16
Torso	LJC to SJC	L5S1	F	SJC - L5S1	30.4	-4.46	67.91	32
			M		+2.9	-2.09	-9.85	-2
Head & Neck	SJC to HV	SJC	F	18.26	6.7	-12.06	69.26	25.6
			M	-0.42	+0.0	-2.15	-3.55	-0.3
Upper Arm	SJC to EJC	SJC	F	18.43	4.4	-7.3	-45.4	33
			M	+0.34	+0.4	+9.0	+0.4	-1
Forearm	EJC to WJC	EJC	F	14.60	2.6	1.9	2.1	14
			M	+0.50	+0.8	-0.5	-1.1	-3
Hand	WJC to mid MH2-MH5	WJC	F	4.28	1.0	4.8	7.7	43
			M	+0.21	+0.2	+2.6	+0.5	-5

and accelerations:

$$\boldsymbol{V}_i = \boldsymbol{Ad}_{\boldsymbol{g}_{i-1,i}^{-1}}(\boldsymbol{V}_{i-1}) + \boldsymbol{\xi}_i\dot{\theta}_i \tag{3}$$

$$\dot{\boldsymbol{V}}_i = Ad_{\boldsymbol{g}_{i-1,i}^{-1}}\left(\dot{\boldsymbol{V}}_{i-1}\right) + \boldsymbol{\xi}_i\ddot{\theta}_i + \boldsymbol{ad}_{\boldsymbol{Ad}_{\boldsymbol{g}_{i-1,i}^{-1}}(\boldsymbol{V}_{i-1})}\left(\boldsymbol{\xi}_i\dot{\theta}\right) \tag{4}$$

2) Backward Propagation: The contact wrench at joint i can be expressed as the vector $\boldsymbol{\Gamma}_i$. Two wrenches can be related through the transpose of $\boldsymbol{ad}$ and $\boldsymbol{Ad}$ which are written as $\boldsymbol{ad}^T$ and $\boldsymbol{Ad}^T$:

$$\boldsymbol{\Gamma}_i = \boldsymbol{Ad}^{\star}_{\boldsymbol{g}_{i,i+1}^{-1}}\boldsymbol{\Gamma}_{i+1} \tag{5}$$

The wrenches at each joint can then be found via a backwards recursion step:

$$\boldsymbol{\Gamma}_i = \boldsymbol{Ad}^T_{\boldsymbol{g}_{i,i+1}^{-1}}\boldsymbol{\Gamma}_{i+1} + \boldsymbol{\mathcal{I}}_i\dot{\boldsymbol{V}}_i - \boldsymbol{ad}^T_{\boldsymbol{V}_i}(\boldsymbol{\mathcal{I}}_i\boldsymbol{V}_i) + \boldsymbol{\Gamma}_{\boldsymbol{E},i} \tag{6}$$

where $\boldsymbol{\Gamma}_{\boldsymbol{E},i}$ are any external wrenches acting on that link, and $\boldsymbol{\mathcal{I}}_i$ is the effective matrix of inertia for the segment i rotating about joint i. Using the notation in Table I, this matrix can be written as:

$$\boldsymbol{\mathcal{I}}_i = \begin{bmatrix} m_i \cdot \mathbb{I} & -m_i\hat{\boldsymbol{r}}_i \\ m_i\hat{\boldsymbol{r}}_i & m_i\phi_i^2 - m_i\hat{\boldsymbol{r}}^2 \end{bmatrix} \tag{7}$$

where $\boldsymbol{r}_i$ and ϕ_i are the the centre of mass and the radius of gyration for segment i.

D. L5S1 Vertebral Model

While the computation of the wrench at each joint is sufficient in systems that can exert a pure torque, in biological systems the joint torques found through inverse dynamics need to be related to muscular forces. These muscular forces are linked with the linear components of the wrench to find the true loading at the joint.

The sagittal low-back model developed by Chaffin [4] is used to estimate the shear and normal forces at the L5-S1 joint. This model includes the effects of the posterior muscles of the spine and Intra-Abdominal Pressure (P_A, Figure 1).

The role of the Intra-Abdominal Pressure (IAP) on muscular forces is modelled based on the relationship from Morris and Fisher [49], linking the hip angle θ_H (deg.), moment at the Lumbar Joint Centre (LJC) τ_{LJC} (Nm), and expected IAP (Pa):

$$P_A = 0.133\left(43 - 0.36\left(\tilde{\theta}_{HJC}\right)\right)\tau_{LJC} \tag{8}$$

with the adjusted hip angle defined as:

$$\tilde{\theta}_{HJC} = \theta_{HJC} + a\sin\left(\frac{l_T}{l_B}\sin\left(\theta_{LJC}\right)\right) \tag{9}$$

where l_T and l_B are the distances between the LJC and SJC, and the HJC and SJC respectively. The abdominal pressure is then converted into a force using the non-scaled diaphragm area of $46.5\times10^{-3}m^2$ and an effective moment arm of 70 mm [4].

Muscular forces are then estimated from the remainder torque. A moment arm of 6.5 cm is used based on standard conventions [4]. The lumped muscular force F_M can therefore be written explicitly:

$$0.065F_M = \tau_{LJC} - 0.070 \cdot 46.5 \times 10^{-3}P_A \tag{10}$$

The total compression and shear forces in the lumbar frame at the LJC ($\boldsymbol{\sigma}_{L5}$) can then be written as:

$$\boldsymbol{\sigma}_{L5} = \begin{bmatrix} \sigma_{shear} \\ \sigma_{comp.} \end{bmatrix} = \begin{bmatrix} F_{Y,LJC} \\ F_{Z,LJC} + F_M - 46.5 \times 10^{-3}P_A \end{bmatrix} \tag{11}$$

Where $F_{Y,LJC}$ and $F_{Z,LJC}$ are the linear Y and Z axis forces from the $\boldsymbol{\Gamma}_{LJC}$ body wrench.

These estimated vertebral forces at L5 are then rotated forward by (-40 deg) to lie along the the estimated sacral cutting

plane [4]. This gives an estimate for the compression and shear forces at S1 ($\boldsymbol{\sigma}_{S1}$).

E. Secondary Metrics

Through this inverse dynamic analysis, it is possible to obtain a number of secondary metrics at the joint and body levels. The computations for these derived metrics are given:

1) Joint Power: This is estimated for each frame based on the computed angular velocity and torque values.

$$P_i = \tau_i \omega_i \tag{12}$$

2) Joint Work: Two work values are computed for each joint, corresponding to the total energy that the joint adds and removes from the system. These are computed as the trapezoidal integral of the the positive and negative components of joint power.

3) Torso Momenta and Kinetic Energy: These values are computed from the body velocities of the torso and the torso inertia tensor $\mathcal{I}_{torso}$.

$$\boldsymbol{p} = \boldsymbol{I}_{torso} \boldsymbol{V}^b_{torso}$$

$$K.E. = \boldsymbol{V}^{b^T}_{torso} \boldsymbol{I}_{torso} \boldsymbol{V}^b_{torso} \tag{13}$$

These are transformed from the torso body frame into the world frame for analysis.

4) STS Time: A variation on a standard clinical measure, the time taken to perform the STS action is computed as time between *quiet* sitting and standing. Quiet sitting and standing are defined as states where the subject is in the seated or standing positions and the torso kinetic energy is approximately zero.

5) Dynamic SVA: A variation on a standard radiographic measure, the dynamic SVA is taken to be the peak horizontal distance between the SJC and the HJC in the saggital plane.

III. Experimental Validation

A. Experimental Protocol

Ten subjects (3F/7M, age: 30.9 $\pm$ 9.6, height: 1.76 $\pm$ 0.12 m, mass: 67.4 $\pm$ 11.2 kg) were recruited under informed consent (UCSF IRB 16-21015). Subjects wore close fitting exercise clothing (sports bra, exercise shorts). The chair height was adjusted so that the subject's thighs were parallel to the floor with their knees directly above their ankles during natural sitting (Figure 2). Subjects were asked to perform STS with their arms folded across their chest, hands touching the opposite elbow. The standing action was otherwise non-coached with subjects performing the action naturally. Three trials, each consisting of three STS, were recorded for each subject.

B. Active Motion Capture Model

An 8-camera active motion capture system (Phasespace, Impulse X2) provides a ground-truth estimate of position and orientation of each body segment. A force platform (AMTI, OPT464508-1000) was used to measure the ground reaction forces at the feet. A custom chair was built and instrumented with a six-axis force sensor (ATI, Omega 160) to measure the contact forces during seat contact. The Kinect, motion-capture

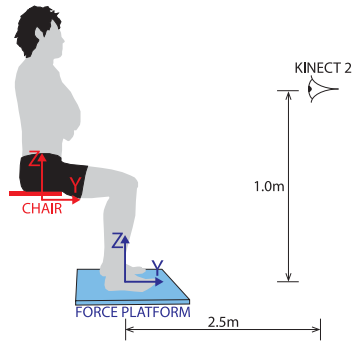

Fig. 2. Cartoon of the experimental setup showing coordinate frames used for the force platform, chair force, and Kinect location.

and force platform were synchronised temporally via. network time protocol (NTP), re-calibrated, and zeroed before each experiment. The Phasespace and Kinect systems were synchronised spatially using a chessboard with attached motion capture markers. Motion and force data were simultaneously recorded from the Kinect 2 (30 Hz), motion capture system (480 Hz) and force sensors (1 kHz), and time-stamped. The Kinect camera was located 2.5 meters directly in-front of the subject, and 1 m vertically from the subjects feet.

Thirty-two LED markers were position on the subject's skin using adhesive Velcro based on the Plug-in-Gait markers set [50] (Figure 3). Additional markers were placed on the medial elbow, knee, and ankle positions to allow for estimates of joint centre from the medio-lateral marker pairs. In cases where the subject's shorts or sports bra obscured the ASIS, PSIS, or XP landmarks, a clip was used to secure the marker to clothing at the desired landmark.

In addition to the STS protocol, a dataset was collected for identifying the functional joint centres for each segment based on the Recap2 protocol [51]. Subjects were asked to move each joint through its full range of motion three times. The Recap2 protocol was only used to find the functional centres for the ground truth motion capture model. The rigid-body model for the lower limbs and torso used for each each segment are shown in Figure 3. The coordinate system is based on Wu [52], with the exception of the pelvis segment where the origin is located at the midpoint of the ASIS and PSIS markers.

Geometric sphere fitting was used to find the hip joint centre based on the recommendation by the ISB [52] as all subjects were able to move sufficiently [53]. The inter-malleolar point was selected for the ankles from Wu [52], the inter-epicondyle point for the knee [54], and L5/S1 from an allometrically scaled pelvic model [55]. The recovered joint-centres were planarised and the relative angles were determined at each frame.

C. Ground and Seat Reaction Forces

The model assumes a single point of contact at the ankles. During the seated portion of the STS action, the subject is not modelled as being in contact with a chair due to the lack of an estimated chair contact point. To allow for comparison between the model and the observed contact forces, the wrench

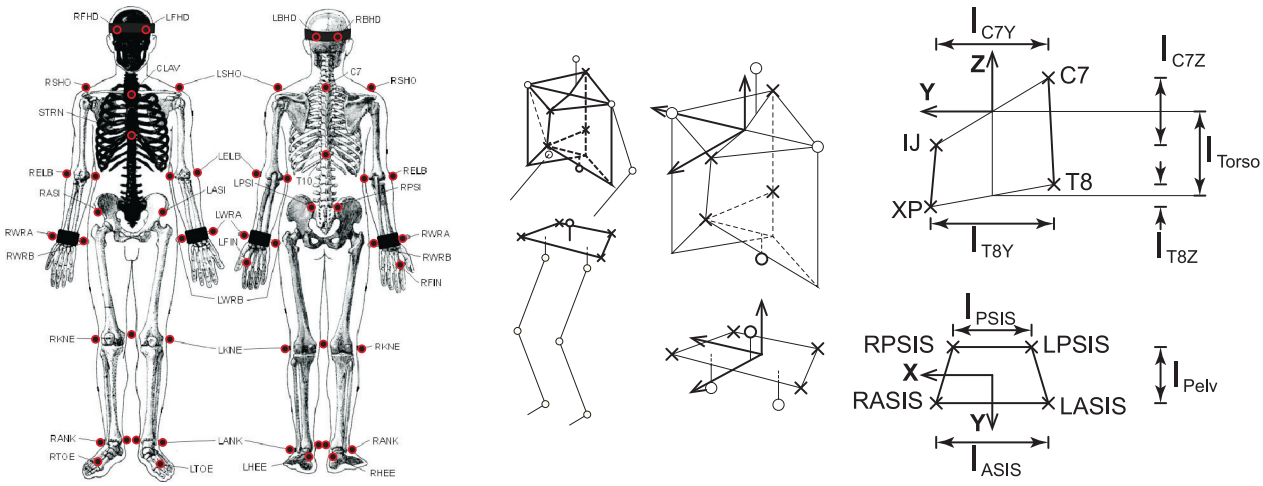

Fig. 3. Left: Motion capture marker protocol. Markers (red) are shown superimposed on the standard Plug-in-Gait model (original image modified from [50]). Centre: Rigid-body frames used for the validation model. Torso and pelvis frames are highlighted with markers shown as crosses and joint centres shown as circles. Right: Segment-marker definitions used for NLS recovery. The sagittal view of the torso frame and caudal view of the pelvis frame are shown. Torso markers were located at the Incisura jugularis sternalis (IJ), Xiphoid Process (XP), and at the C7 and T8 spinous processes which were found during standing. Pelvis markers were located at the right and left Anterior Superior Iliac Spines (ASIS) and Posterior Superior Iliac Spines (PSIS).

measured at the chair was transformed into the force platform frame to provide a single total wrench. Using the notation from Section II-C2, the wrench at the chair and force platform ($\mathbf{\Gamma}_{chair}$ and $\mathbf{\Gamma}_{FP}$) can be combined to give the total contact wrench in the force platform frame $\mathbf{\Gamma}_{Total}$:

$$\mathbf{\Gamma}_{Total} = \mathbf{\Gamma}_{FP} + \boldsymbol{Ad}^{T}_{\boldsymbol{g}^{-1}_{FP,chair}} \mathbf{\Gamma}_{chair} \tag{14}$$

This conversion allows for a direct comparison between the estimated ground reaction forces and the measurements from the force platform and the chair.

D. Data Analysis

All data processing was performed offline on Kinect 2 joint centre data. An Intel i7-5820K processor with 32GB RAM running Windows 7 Enterprise was used. Each trial consisted of roughly 880 frames of data which was post-processed at 25 $\pm$ 2 fps. Neither a graphics card nor parallelisation framework were used to aid computation.

Three measures were used to assess the recovered state trajectories and metrics:

1) Mean Absolute Error (MAE): error between two signals

2) Lin's Concordance Correlation Coefficient (CCC): assesses inter-rater reliability between methods

3) Inter-class Correlation Coefficient (ICC): identifies the absolute agreement (ICC(2,1)) and relative consistency (ICC(3,1)) between methods [56]–[58]. ICC values were interpreted as poor (<0.4), fair ($0.4-0.59$), good ($0.6-0.74$), and excellent (≥ 0.75) based on the treatment by [59], [60].

IV. Results

The performance of the proposed depth camera dynamic assessment system is separated into three components. First, the ground reaction forces (GRF) estimated using the depth camera model and the gold-standard motion capture model are separately evaluated against the measured contact forces in Table II. Then, the proposed model is evaluated against the gold-standard model for a selection of joint and body variables (Tables III, IV). Finally, a selection of peak metrics are provided in Table V. These metrics represent potential assessment measures for the STS action, including but not limited to existing measures used in patient assessment and occupational health. Trajectory plots for a representative subject are given in Figure 4 showing ground reaction forces, joint torques, and estimated joint powers, and Figure 5 showing the torso momenta and vertebral loads at the LJC.

The proposed depth camera method performed comparably to the baseline active motion capture model in the recovery of the ground reaction forces (Table II, Figure 4 (left)). Both the linear forces and torque were found to have similar range and MAE compared to the total wrench computed from the force platform and instrumented chair. Both models were found to have excellent concordance in estimating the vertical force and torque. As the centre of pressure can be estimated from these two values, excellent concordance was also found for the centre of pressure. In contrast, the horizontal force was found to have relatively poorer concordance.

The estimated joint torques and powers from the proposed method were found to have excellent concordance with those estimated from the baseline model. An exception to this was the estimated ankle power, which has poor concordance, agreement, and consistency when compared with the baseline model.

The trajectories of the body parameters show in Table IV show excellent concordance for all measures including measures of posture, momenta, and low-back vertebral loading. The negative values seen for vertical and angular momenta correspond to the initial forward flexion of the torso, with the subsequent rise and straightening of the torso seen in the corresponding positive

TABLE II
VALIDATION OF THE ESTIMATED GROUND REACTION USING BASELINE (GOLD STANDARD MOTION CAPTURE) AND PROPOSED (KINECT 2) MODELS AGAINST THE TOTAL CONTACT WRENCH MEASURED FROM THE FORCE PLATFORM AND INSTRUMENTED FORCE CHAIR

Metric	Method	Range	MAE	CCC	ICC(2,1)	ICC(3,1)
Force Y (N)	Baseline	-79.8 to 99.9	26.1 ± 31.5	0.652	0.652	0.667
	Proposed	-88.8 to 95.8	26.2 ± 24.3	0.757	0.757	0.757
Force Z (N)	Baseline	552.7 to 799.8	32.4 ± 40.5	0.941	0.941	0.941
	Proposed	509.4 to 826.9	34.1 ± 36.4	0.949	0.949	0.949
Torque (Nm)	Baseline	-254.5 to 48.0	28.5 ± 35.7	0.921	0.921	0.929
	Proposed	-262.5 to 57.3	32.9 ± 29.2	0.929	0.929	0.935
Centre of Pressure (cm)	Baseline	-38.3 to 7.10	4.11 ± 4.54	0.933	0.933	0.940
	Proposed	-39.0 to 10.2	4.89 ± 4.06	0.930	0.930	0.936

TABLE III
VALIDATION OF JOINT TRAJECTORY PARAMETERS OBTAINED FROM THE PROPOSED METHOD AGAINST THE BASELINE ACTIVE MOTION CAPTURE MODEL

Metric	Joint	Range	MAE	CCC	ICC(2,1)	ICC(3,1)
Joint Torques / $(H^2 \cdot M)$ $(1/s^2)$ $(\times 10^{-3})$	**Ankle**	-1142 to 281	139 ± 13	0.937	0.937	0.937
	Knee	-1310 to 47	87 ± 80	0.969	0.969	0.971
	Hip	-206 to 533	83 ± 80	0.894	0.894	0.917
	L5S1	-126 to 440	61 ± 63	0.886	0.887	0.916
Joint Powers / $(H^2 \cdot M)$ $(1/s^3)$ $(\times 10^{-3})$	**Ankle**	-106 to 334	8 ± 9	0.380	0.380	0.392
	Knee	-142 to 1000	15 ± 17	0.788	0.788	0.793
	Hip	-444 to 180	7 ± 9	0.820	0.820	0.820
	L5S1	-414 to 287	7 ± 9	0.812	0.812	0.813

TABLE IV
VALIDATION OF BODY TRAJECTORY PARAMETERS OBTAINED FROM THE PROPOSED METHOD AGAINST THE BASELINE ACTIVE MOTION CAPTURE MODEL

Metric	Dimension	Range	MAE	CCC	ICC(2,1)	ICC(3,1)
SVA / Height (dimless) $(\times 10^{-3})$	**Y**	-18 to 143	12 ± 9	0.968	0.968	0.977
Centre of Mass (cm)	**Y**	-37.6 to 3.1	2.8 ± 1.9	0.973	0.973	0.979
	Z	77.9 to 1136.6	1.7 ± 2.0	0.985	0.985	0.987
Torso Momenta / $(H \cdot M)$ (1/s) $(\times 10^{-3})$	**Y**	0 to 157	15 ± 13	0.923	0.923	0.925
	Z	-51 to 219	23 ± 26	0.912	0.912	0.913
Torso Momenta / $(H^2 \cdot M)$ (1/s) $(\times 10^{-3})$	**Angular**	-44 to 16	5 ± 5	0.937	0.937	0.937
Lumbar Loads / $(H \cdot M)$ $(1/s^2)$	**Shear**	-2.254 to 0.427	0.235 ± 0.243	0.926	0.926	0.935
	Normal	2.219 to 11.787	0.963 ± 1.248	0.879	0.879	0.901
Sacral Loads / $(H \cdot M)$ $(1/s^2)$	**Shear**	1.316 to 5.106	0.351 ± 0.438	0.900	0.900	0.901
	Normal	1.758 to 10.610	0.903 ± 1.130	0.886	0.886	0.901

TABLE V
CANDIDATE PEAK METRICS FOR ASSESSMENT OF STS ACTIONS PROPOSED VS. BASELINE

Metric	Typical Value	Range	MAE	CCC	ICC(2,1)	ICC(3,1)
STS Time (s)	1.443 ± 0.116	1.17 to 1.73	0.236 ± 0.115	0.258	0.261	0.628
Peak SVA / (H) (no unit) $(\times 10^{-3})$	143 ± 24	94 to 196	13 ± 13	0.697	0.700	0.739
Peak Torso Horizontal Momentum / $(H \cdot M)$ (1/s)	157 ± 21	123 to 223	12 ±14	0.588	0.591	0.604
Peak Torso Vertical Momentum / $(H \cdot M)$ (1/s)	219 ± 27	176 to 287	31 ± 22	0.335	0.338	0.563
Peak Torso Flex Momentum / $(H^2 \cdot M)$ (1/s)	-44 ± 6	-65 to -31	3 ± 4	0.495	0.499	0.516
Peak Torso Extend Momentum / $(H^2 \cdot M)$ (1/s)	16 ± 6	6 to 31	3 ± 2	0.787	0.789	0.872
Peak KJC Extension Torque / $(H^2 \cdot M)$ $(1/s^2)$ $(\times 10^{-3})$	1310 ± 135	1020 to 1619	45 ± 44	0.889	0.890	0.896
Peak HJC Extension Torque / $(H^2 \cdot M)$ $(1/s^2)$ $(\times 10^{-3})$	533 ± 107	351 to 770	80 ± 59	0.632	0.635	0.668
Peak HJC Flexion Torque / $(H^2 \cdot M)$ $(1/s^2)$ $(\times 10^{-3})$	206 ± 82	251 to 379	78 ± 38	0.573	0.576	0.870
Peak LJC Extension Torque / $(H^2 \cdot M)$ $(1/s^2)$ $(\times 10^{-3})$	126 ± 59	32 to 255	36 ± 23	0.703	0.706	0.821
Peak LJC Flexion Torque / $(H^2 \cdot M)$ $(1/s^2)$ $(\times 10^{-3})$	440 ± 82	309 to 630	73 ± 40	0.594	0.597	0.852
Peak KJC Motoric Power / $(H^2 \cdot M)$ $(1/s^3)$ $(\times 10^{-3})$	1000 ± 235	694 to 1672	164 ± 165	0.463	0.467	0.557
Peak LJC Motoric Power / $(H^2 \cdot M)$ $(1/s^3)$ $(\times 10^{-3})$	287 ± 121	123 to 629	53 ± 48	0.806	0.808	0.853
Peak LJC Braking Power / $(H^2 \cdot M)$ $(1/s^3)$ $(\times 10^{-3})$	414 ± 174	233 to 1254	96 ± 154	0.281	0.284	0.316
Max Sacral Compression Force / $(H \cdot M)$ $(1/s^2)$	10.61 ± 1.09	8.65 to 12.93	1.09 ± 0.62	0.553	0.556	0.823
Min Sacral Compression Force / $(H \cdot M)$ $(1/s^2)$	1.76 ± 0.21	1.38 to 2.4	0.12 ± 0.09	0.702	0.704	0.725
Max Sacral Posterior Shear Force / $(H \cdot M)$ $(1/s^2)$	5.11 ± 0.42	4.28 to 6.19	0.27 ± 0.18	0.788	0.790	0.796
Min Sacral Posterior Shear Force / $(H \cdot M)$ $(1/s^2)$	1.32 ± 0.16	0.90 to 1.67	0.13 ± 0.09	0.397	0.400	0.400

values. The link between the torso momenta and the vertebral forces at the LJC are shown for a representative subject in Figure 5. The peak LJC load is seen at $t = 0.8$ s which corresponds to the forward deceleration and vertical acceleration of the torso.

V. DISCUSSION

The proposed single depth camera system was found to be comparable to the baseline active motion capture model and measured contact forces. Concordance and correlation coeffi-

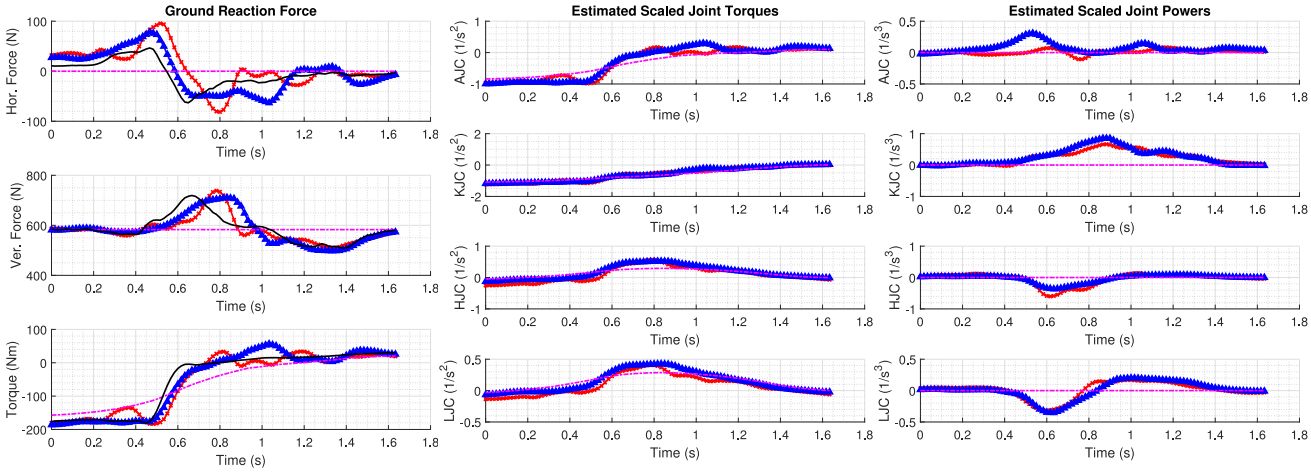

Fig. 4. Comparison of the proposed method and the baseline model on the recovery of ground reaction forces and joint states for a representative subject. Left: Ground reaction forces. The total wrench measured by the force platform and chair are shown as a solid black line. Middle: Estimated joint torques. Right: Estimated joint powers. The proposed method and baseline models are shown as blue triangles and red crosses respectively. A quasi-static method is also presented (magenta dotted line) to highlight the effect of including dynamics into modelling approach.

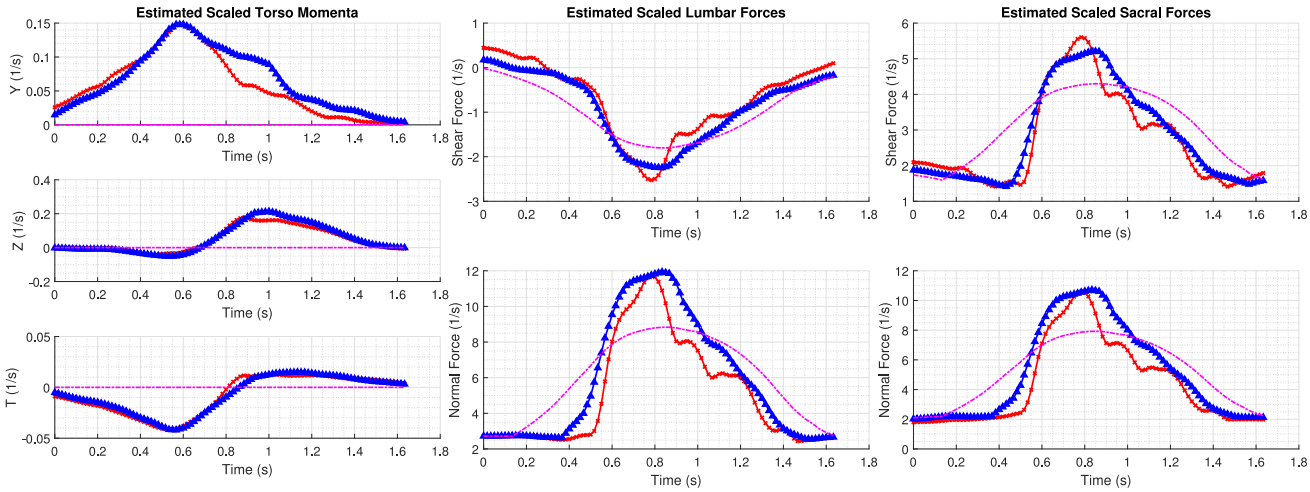

Fig. 5. Comparison of the proposed method and the baseline model on the recovery of body momenta and LJC forces for a representative subject. Left: Torso momenta as viewed in the world frame. Middle: Estimated LJC forces in the L5 frame. Right: Estimated LJC forces in the S1 frame. The proposed method and baseline models are shown as blue triangles and red crosses respectively. A quasi-static method is also presented (magenta dotted line) to highlight differences in using a dynamic modelling approach.

cients were found to be excellent (≥ 0.75) for all contact forces and the identified joint and body trajectory measures, with the exception of ankle power. The concordance was found to be high for the ground reaction vertical force and torque. The correlation coefficients were found to be lower for the horizontal force using both methods. The lack of a rise in consistency in the horizontal force suggests that this decline cannot be attributed to a simple offset, but a difference in the overall shape of the horizontal force curves. This is likely due to the increased importance of the modelled dynamic effects in estimating horizontal force compared to the vertical and torque values and the increased complexity of the motion in the horizontal plane. The estimated ground reaction forces for the proposed and baseline models are shown in Figure 4. While the range spanned by each of these measurements and the associated MAEs are comparable, the overall shape of the recovered curves are visually different for horizontal force when compared to the vertical force and torque.

The decreased performance in concordance, agreement, and consistency for ankle power may be caused by the compounding of error in the estimates of angular velocity and torque, combined with the relatively lower observed range of joint velocities in the STS action. This may be exacerbated by the underlying choice of sensor and processing method used in the proposed method. The raw Kinect 2 skeleton has poor joint position estimates for the lower limbs. While this is improved using a rigid-body model, inaccuracies in this underlying data could propagate into the estimates of ankle and knee velocities. This could also be an explanation for knee where the relatively high CCC value for joint torque is contrasted by a lower value for joint power.

The estimated torques at the knee and hip can be compared with the literature. Peak knee and hip extension torques of 1.08–1.25 and 0.73–0.98 $\mathrm{Nm}/(\mathrm{M}\cdot\mathrm{H})$ respectively have been reported for healthy young subjects [42]–[44], [61]. Accounting for the change in scaling factor, the peak extension torque was 0.938 $\mathrm{Nm}/(\mathrm{M}\cdot\mathrm{H})$ for the hip using the proposed depth camera method. For a comparison of peak knee extension torques, the point of seat-off needs to be estimated. Using the time of peak horizontal momentum as the moment of seat off, the corresponding peak knee extension torque of 1.23 $\mathrm{Nm}/(\mathrm{M}\cdot\mathrm{H})$ can be found, agreeing with the value found by Mak [44]. The hip flexion values found by Mak are lower than in our sample (0.362 $\mathrm{Nm}/(\mathrm{M}\cdot\mathrm{H})$). Healthy elders, and elders with Parkinson's disease were found to have peak hip flexion values of 0.201 and 0.089 $\mathrm{Nm}/(\mathrm{M}\cdot\mathrm{H})$ respectively. This discrepancy could be due to differences in experimental population as subjects in Mak's study were 38 years older.

A selection of candidate assessment metrics is presented in Table V. These metrics consist of measures similar to conventional clinical measures (STS time, peak SVA), and those that have been identified as being biomechanically relevant.

The importance of performing full dynamic analysis when recovering lumbar loads is shown in Figures 4 and 5. By neglecting the role of segment inertiae, the observed peak shear and compression loads at L5 and S1 are underestimated, there is no variation in linear ground reaction forces, and joint power and body momenta cannot be estimated.

The computation rate of 25 fps in this current implementation is below real time; a number of code improvements such as conversion from MATLAB to C++ would lead to faster run times. These processing steps could be performed in parallel as each frame is effectively decoupled after the joint velocities and accelerations have been recovered.

VI. Conclusion

This paper presents a method for extracting quantitative performance measures from a rapid, commonly used clinical test. This method was found to provide comparable estimates of ground reaction forces, joint torques, and body momenta when compared to a baseline active motion-capture model and instrumented force sensors. As only a single depth camera is used, the time required to setup and collect movement data is extremely fast, without the need to calibrate and synchronise a multi-camera setup and force sensors. No surface markers or calibration actions are needed allowing for rapid patient testing without significant additional training. The proposed system is therefore presented as an inexpensive and feasible augmentation to the current FT-STS test already used in clinical practice. While the implementation tested in this paper used angular states recovered from a rigid-body depth camera system, the dynamic and musculoskeletal models could be adapted for use with alternative camera systems, or sensors such as inertial measurement units.

A. Limitations

While the system has been shown to be capable of providing an accurate assessment of the biomechanical states during sit-to-stand, there are a number of limitations and modelling assumptions. This paper presents validation on a relatively small, homogeneous, cohort of ten asymptomatic subjects. While this study shows an initial validation of the proposed system, a larger study consisting of more heterogeneous subjects, especially specific clinical populations is needed. The low back rhythm and vertebral model generated on these control subjects is assumed to translate to clinical subjects. Depending on the clinical population, the assumption of a single point joint at the low back may not be appropriate. The patients arms are not tracked and modelled in this system. If patients require the use of chair arm rests, or arm swing to generate sufficient momentum to stand, the proposed dynamic model will need to be expanded to track upper limb movement. Similarly, any significant motion outside of the sagittal plane, such as asymmetric loading of the legs will break the sagittal modelling assumption. Performing this modelling and analysis in 3D may better capture these asymmetries, improving the validity of this approach in subjects with abnormal movement patterns. This system is currently being tested in clinic on subjects with low back pain, and during recovery from spinal fusion. By repeating some of these underlying analyses on clinical subjects, the limitations of these assumptions and necessary improvements can be identified.

Appendix
Lie Group Notation

This paper uses Lie Group formulations to model the subject and perform inverse dynamics. This section summarises some key concepts and notation for completeness. Full discussion on this approach to rigid-body modelling can be found in geometric robotic literature [26], [48].

Every rigid-body transformation can be represented by the homogenous matrix $\boldsymbol{g}_{A,B}$:

$$\boldsymbol{g}_{A,B} = \begin{bmatrix} \boldsymbol{R}_{A,B} & \boldsymbol{q}_{A,B} \\ \boldsymbol{0} & 1 \end{bmatrix} \tag{15}$$

where $\boldsymbol{R}_{A,B}$ and $\boldsymbol{q}_{A,B}$ are the rotation and translation components of the transformation. The rotation matrix and the homogeneous transformation matrix are elements of the special orthogonal ($\mathcal{SO}$) and special Euclidean ($\mathcal{SE}$) Lie groups. These Lie groups have the associated Lie algebras ($\mathfrak{so}$) and ($\mathfrak{se}$). In 3D this the Lie algebra can be parameterised by the vectors $\boldsymbol{\omega} \in \mathbb{R}^3$ and $\boldsymbol{V} \in \mathbb{R}^6$ where:

$$\hat{\boldsymbol{\omega}} = \begin{bmatrix} 0 & -\omega_3 & \omega_2 \\ \omega_3 & 0 & -\omega_1 \\ -\omega_2 & \omega_1 & 0 \end{bmatrix} \hat{\boldsymbol{V}} = \begin{bmatrix} \hat{\boldsymbol{\omega}} & \boldsymbol{v} \\ \boldsymbol{0} & 1 \end{bmatrix} \tag{16}$$

and

$$\boldsymbol{R} = \boldsymbol{R}_0 e^{\hat{\boldsymbol{\omega}}} \qquad \boldsymbol{g} = \boldsymbol{g}_0 e^{\hat{\boldsymbol{V}}} \tag{17}$$

where $\boldsymbol{R} \in \mathcal{SO}(3)$ and $\boldsymbol{g} \in \mathcal{SE}(3)$.

This allows for two matrix forms of adjoint operator: $\boldsymbol{ad}$ and $\boldsymbol{Ad}$ which are parameterised by an element of the Lie algebra

and Lie group respectively:

$$ad_{V_1}(V_2) = \begin{bmatrix} \hat{\omega}_1 & \hat{v}_1 \\ 0 & \hat{\omega}_1 \end{bmatrix} V_2$$

$$Ad_{g_1}(V_2) = \begin{bmatrix} R_1 & \hat{q}_1 R_1 \\ 0 & R_1 \end{bmatrix} V_2 \quad (18)$$

ACKNOWLEDGMENT

The authors would like to thank Patrick Curran and Gregorij Kurillo for their assistance in the data collection process and Oliver O'Reilly for his advice and discussion on the dynamic metrics.

REFERENCES

[1] J. Buckup, *Clinical tests for the musculoskeletal system: Examinations, signs, phenomena*. Thieme, Stuttgart, 2008.
[2] J. T. McConville, C. E. Clauser, T. D. Churchill, J. Cuzzi, and I. Kaleps, "Anthropometric relationships of body and body segment moments of inertia," *Anthropology Research Project Inc.*, Yellow Springs, OH, 1980.
[3] J. Young, R. F. Chandler, C. C. Snow, K. Robinette, G. Zehner, and M. Lofberg, "Anthropometric and mass distribution characteristics of the adult female," Civil Aerospace Med. Inst., USA, Tech. Rep. FAA-AM-83-16, 1983.
[4] D. B. Chaffin, G. B. J. Andersson, and B. J. Martin, *Occupational Biomechanics*, Hoboken: Wiley-Interscience, 2006.
[5] R. Dumas, L. Chèze, and J. P. Verriest, "Adjustments to McConville *et al.* and Young *et al.* body segment inertial parameters," *J. Biomechanics*, vol. 40, no. 3, pp. 543–553, 2007.
[6] G. Venture, K. Ayusawa, and Y. Nakamura, "Motion capture based identification of the human body inertial parameters," in *Proc. Annu. Int. Conf. IEEE Eng. Med. Biol. Soc.*, 2008, vol. 2008, no. 3, pp. 4575–4578. [Online]. Available: http://www.ncbi.nlm.nih.gov/pubmed/19163734
[7] K. Ayusawa, G. Venture, and Y. Nakamura, "Real-time implementation of physically consistent identification of human body segments," in *Proc. - IEEE Int. Conf. Robotics Autom.*, 2011, pp. 6282–6287.
[8] D. G. Lloyd and T. F. Besier, "An EMG-driven musculoskeletal model to estimate muscle forces and knee joint moments in vivo," *J. Biomechanics*, vol. 36, no. 6, pp. 765–776, 2003.
[9] E. A. Clancy, O. Bida, and D. Rancourt, "Influence of advanced electromyogram (EMG) amplitude processors on EMG-to-torque estimation during constant-posture, force-varying contractions," *J. Biomechanics*, vol. 39, no. 14, pp. 2690–2698, 2006.
[10] J. Rasmussen, V. Vondrak, M. Damsgaard, M. D. Zee, and Z. Dostal, "The anybody project computer analysis of the human body," *Biomechanics Man*, pp. 270–274, 2002.
[11] S. L. Delp *et al.*, "OpenSim: Open source to create and analyze dynamic simulations of movement," *IEEE Trans. Bio-Med. Eng.*, vol. 54, no. 11, pp. 1940–1950, 2007.
[12] M. Csuka and D. J. McCarty, "Simple method for measurement of lower extremity muscle strength," *Amer. J. Med.*, vol. 78, no. 1, pp. 77–81, 1985.
[13] Q. Wang, W. Chen, A. A. Timmermans, C. Karachristos, J. B. Martens, and P. Markopoulos, "Smart rehabilitation garment for posture monitoring," in *Proc. Annu. Int. Conf. IEEE Eng. Med. Biol. Soc. (EMBS)*, 2015, pp. 5736–5739.
[14] G. D. Voinea, S. Butnariu, and G. Mogan, "Measurement and geometric modelling of human spine posture for medical rehabilitation purposes using a wearable monitoring system based on inertial sensors," *Sensors (Basel)*, vol. 17, no. 1, pii: E0003, 2017.
[15] X. Yan, H. Li, A. R. Li, and H. Zhang, "Wearable IMU-based real-time motion warning system for construction workers' musculoskeletal disorders prevention," *Autom. Construction*, vol. 74, pp. 2–11, Feb. 2017. [Online]. Available: https://www.sciencedirect.com/science/article/pii/S0926580516303314
[16] W. S. Marras, F. A. Fathallah, R. J. Miller, S. W. Davis, and G. A. Mirka, "Accuracy of a three-dimensional lumbar motion monitor for recording dynamic trunk motion characteristics," *Int. J. Ind. Ergonom.*, vol. 9, no. 1, pp. 75–87, 1992.
[17] W. S. Marras *et al.*, "The quantification of low back disorder using motion measures: Methodology and validation," *Spine*, vol. 24, no. 20, pp. 2091–2100, 1999.
[18] W. S. Marras, S. A. Ferguson, D. Burr, K. G. Davis, and P. Gupta, "Spine loading in patients with low back pain during asymmetric lifting exertions," *Spine J.*, vol. 4, no. 1, pp. 64–75, 2004.
[19] R. Poppe, "Vision-based human motion analysis: An overview," *Comput. Vis. Image Understanding*, vol. 108, no. 1-2, pp. 4–18, 2007.
[20] Z. Zhang, "Microsoft Kinect sensor and its effect," *IEEE Multimedia*, vol. 19, no. 2, pp. 4–10, 2012.
[21] Q. Wang, G. Kurillo, F. Ofli, and R. Bajcsy, "Evaluation of pose tracking accuracy in the first and second generations of Microsoft Kinect," *Proc. 2015 IEEE Int. Conf. Healthcare Inform.*, pp. 380–389.
[22] J. K. Nichols, M. P. Sena, J. L. Hu, O. M. OReilly, B. T. Feeley, and J. C. Lotz, "A Kinect-based movement assessment system: Marker position comparison to Vicon," *Comput. Methods Biomechanics Biomed. Eng.*, vol. 20, no. 12, pp. 1289–1298, 2017. [Online]. Available: https://doi.org/10.1080/10255842.2017.1340464
[23] M. Ding and G. Fan, "Articulated and generalized Gaussian kernel correlation for human pose estimation," *IEEE Trans. Image Process.*, vol. 25, no. 2, pp. 776–789, 2016.
[24] L. Shuai, C. Li, X. Guo, B. Prabhakaran, and J. Chai, "Motion capture with ellipsoidal skeleton using multiple depth cameras," *IEEE Trans. Vis. Comput. Graphics*, vol. 23, no. 2, pp. 1085–1098, 2017.
[25] G. Pavlakos, X. Zhou, K. G. Derpanis, and K. Daniilidis, "Coarse-to-fine volumetric prediction for single-image 3D human pose," in *Proc. 30th IEEE Conf. Comput. Vis. Pattern Recog.*, 2017, pp. 1263–1272.
[26] S. Park, J. Hwang, and N. Kwak, "3D human pose estimation using convolutional neural networks with 2D pose information," in *Proc. Eur. Conf. Comput. Vis. (ECCV) Workshop*, 2016, pp. 156–169.
[27] X. Zhou, X. Sun, W. Zhang, S. Liang, and Y. Wei, "Deep kinematic pose regression," in *European Conference on Computer Vision*, Springer, Cham., pp. 186–201, 2016.
[28] D. Mehta *et al.*, "VNect: Real-time 3D human pose estimation with a single RGB camera," *ACM Trans. Graphics*, vol. 36, no. 4, pp. 1–14, 2017.
[29] P. Zhang, K. Siu, J. Zhang, C. K. Liu, and J. Chai, "Leveraging depth cameras and wearable pressure sensors for full-body kinematics and dynamics capture," *ACM Trans. Graphics*, vol. 33, no. 6, pp. 1–14, 2014.
[30] S. Corazza, L. Mündermann, A. M. Chaudhari, T. Demattio, C. Cobelli, and T. P. Andriacchi, "A markerless motion capture system to study musculoskeletal biomechanics: Visual hull and simulated annealing approach," *Ann. Biomed. Eng.*, vol. 34, no. 6, pp. 1019–1029, 2006.
[31] F. C. Anderson and M. G. Pandy, "Dynamic optimization of human walking," *J. Biomechanical Eng.*, vol. 123, no. 5, p. 381, 2001.
[32] P. Plantard, A. Muller, C. Pontonnier, G. Dumont, H. P. Shum, and F. Multon, "Inverse dynamics based on occlusion-resistant Kinect data: Is it usable for ergonomics?" *Int. J. Ind. Ergonom.*, vol. 61, pp. 71–80, 2017.
[33] P. Plantard, H. P. Hubert, and F. Multon, "Filtered pose graph for efficient Kinect pose reconstruction," *Multimedia Tools Appl.*, vol. 76, no. 3, pp. 4291–4312, 2017.
[34] J. M. Guralnik *et al.*, "Lower extremity function and subsequent disability: Consistency across studies, predictive models, and value of gait speed alone compared with the short physical performance battery," *J. Gerontology*, vol. 55A, no. 4, pp. M221–M231, 2000.
[35] S. Buatois *et al.*, "Five times sit to stand test is a predictor of recurrent falls in healthy community-living subjects aged 65 and older," *J. Amer. Geriatrics Soc.*, vol. 56, no. 8, pp. 1575–1577, 2008.
[36] L. E. Powell and A. M. Myers, "The activities-specific balance confidence (ABC) scale," *J. Gerontology. Series A, Biological Sci. Med. Sci.*, vol. 50A, no. 1, pp. 28–34, 1995.
[37] A. Shumway-Cook and M. Woollacott, *Motor Control: Theory and Practical Applications.* Williams & Wilkins, Philadelphia, 1995.
[38] S. L. Whitney, D. M. Wrisley, G. F. Marchetti, M. A. Gee, M. S. Redfern, and J. M. Furman, "Clinical measurement of sit-to-stand performance in people with balance disorders: Validity of data for the five-times-sit-to-stand test." *Phys. Therapy*, vol. 85, no. 10, pp. 1034–1045, 2005.
[39] P. O. Riley, M. L. Schenkman, R. W. Mann, and W. A. Hodge, "Mechanics of a constrained chair-rise," *J. Biomechanics*, vol. 24, no. 1, pp. 77–85, 1991.
[40] M. A. Hughes, D. K. Weiner, M. L. Schenkman, R. M. Long, and S. A. Studenski, "Chair rise strategies in the elderly," *Clinical Biomechanics*, vol. 9, no. 3, pp. 187–192, 1994.

[41] P. O. Riley, D. E. Krebs, and R. A. Popat, "Biomechanical analysis of failed sit-to-stand," *Trans. Rehabilitation Eng.*, vol. 5, no. 4, pp. 353–359, 1997.
[42] A. B. Schultz, N. B. Alexander, and J. A. Ashton-Miller, "Biomechanical analyses of rising from a chair," *J. Biomechanics*, vol. 25, no. 12, pp. 1383–1391, 1992.
[43] F. Sibella, M. Galli, M. Romei, A. Montesano, and M. Crivellini, "Biomechanical analysis of sit-to-stand movement in normal and obese subjects," *Clinical Biomechanics*, vol. 18, no. 8, pp. 745–750, 2003.
[44] M. K. Mak, O. Levin, J. Mizrahi, and C. W. Hui-Chan, "Joint torques during sit-to-stand in healthy subjects and people with Parkinson's disease," *Clinical Biomechanics*, vol. 18, no. 3, pp. 197–206, 2003.
[45] R. P. Matthew, S. Seko, R. Bajcsy, and J. Lotz, "Kinematic and kinetic validation of an improved rigid bodies," *IEEE J. Biomed. Health Inform.*, 2018. Advance online publication. doi:10.1109/JBHI.2018.2872834.
[46] C. K. Anderson, D. B. Chaffin, and G. D. Herrin, "A study of lumbosacral orientation under varied static loads," *Spine*, vol. 11, no. 5, pp. 456–462, 1986.
[47] S. Seko, R. P. Matthew, R. Bajcsy, and J. C. Lotz, "A functional method for generating individualized spine models from motion-capture data," in *Proc. 2018 40th Annu. Int. Conf. IEEE Eng. Medicine Biol. Soc. (EMBC)*, pp. 1485–1489.
[48] F. C. Park, J. Bobrow, and S. R. Ploen, "A Lie group formulation of robot dynamics," *Int. J. Robotics Res.*, vol. 14, no. 6, pp. 609–618, 1995.
[49] J. M. Morris, D. B. Lucas, and B. Bresler, "Role of the trunk in stability of the spine," *J. Bone Joint Surg.*, vol. 43, no. 3, pp. 327–351, 1961.
[50] Vicon, "The standard Vicon full-body model (Plug-in Gait) marker placement scheme," 2010.
[51] Phasespace, "Recap2 User's Guide," 2010.
[52] G. Wu *et al.*, "ISB recommendation on definitions of joint coordinate system of various joints for the reporting of human joint motion—Part I: Ankle, hip, and spine," *J. Biomechanics*, vol. 35, no. 4, pp. 543–548, 2002. [Online]. Available: http://linkinghub.elsevier.com/retrieve/pii/S0021929001002226
[53] H. Kainz, M. Hajek, L. Modenese, D. J. Saxby, D. G. Lloyd, and C. P. Carty, "Reliability of functional and predictive methods to estimate the hip joint centre in human motion analysis in healthy adults," *Gait Posture*, vol. 53, pp. 179–184, 2017.
[54] T. F. Besier, D. L. Sturnieks, J. A. Alderson, and D. G. Lloyd, "Repeatability of gait data using a functional hip joint centre and a mean helical knee axis," *J. Biomechanics*, vol. 36, no. 8, pp. 1159–1168, 2003.
[55] M. Reed, M. A. Manary, and L. W. Schneider, "Methods for measuring and representing automobile occupant posture," SAE Tech. Paper, Tech. Rep. 724, 1999. [Online]. Available: http://papers.sae.org/1999-01-0959/
[56] P. E. Shrout and J. L. Fleiss, "Intraclass correlations-uses in assessing rater reliability," *Psychological Bulletin*, vol. 86, no. 2, pp. 420–428, 1979.
[57] K. O. McGraw and S. P. Wong, "Forming inferences about some intraclass correlation coefficients," *Psychological Methods*, vol. 1, no. 1, pp. 30–46, 1996.
[58] T. K. Koo and M. Y. Li, "A guideline of selecting and reporting intraclass correlation coefficients for reliability research," *J. Chiropractic Med.*, vol. 15, no. 2, pp. 155–163, 2016. [Online]. Available: http://dx.doi.org/10.1016/j.jcm.2016.02.012
[59] D. V. Cicchetti, "Guidlines, criteria, and rules of thumb for evalauting normed and standardized assessment instruments in psychology," *Psychological Assessment*, vol. 6, no. 4, pp. 284–290, 1994.
[60] M. Eltoukhy, C. Kuenze, J. Oh, and J. Signorile, "Validation of static and dynamic balance assessment using Microsoft Kinect for young and elderly populations," *IEEE J. Biomed. Health Inform.*, vol. 22, no. 1, pp. 147–153, Jan. 2018.
[61] M. M. Gross, P. J. Stevenson, S. L. Charette, G. Pyka, and R. Marcus, "Effect of muscle strength and movement speed on the biomechanics of rising from a chair in healthy elderly and young women," *Gait Posture*, vol. 8, no. 3, pp. 175–185, 1998.